



## Accuracy of small footprint airborne LiDAR in its predictions of tropical moist forest stand structure

G. Vincent <sup>a,\*</sup>, D. Sabatier <sup>a</sup>, L. Blanc <sup>b</sup>, J. Chave <sup>c</sup>, E. Weissenbacher <sup>b</sup>, R. Pélissier <sup>a</sup>, E. Fonty <sup>d</sup>, J.-F. Molino <sup>a</sup>, P. Coutron <sup>a</sup>

<sup>a</sup> IRD, UMR AMAP, Montpellier, 34000 France

<sup>b</sup> CIRAD—UMR Ecofog—Kourou, 97300 France

<sup>c</sup> CNRS/UPS—UMR EDB Toulouse 31000 France

<sup>d</sup> ONF, Direction régionale de la Guyane, Cayenne, 97300 France

### ARTICLE INFO

#### Article history:

Received 21 December 2011

Received in revised form 19 June 2012

Accepted 23 June 2012

Available online 30 July 2012

#### Keywords:

Tropical moist forest

Lidar

Basal area

### ABSTRACT

We predict stand basal area (BA) from small footprint LiDAR data in 129 one-ha tropical forest plots across four sites in French Guiana and encompassing a great diversity of forest structures resulting from natural (soil and geological substrate) and anthropogenic effects (unlogged and logged forests). We use predictors extracted from the Canopy Height Model to compare models of varying complexity: single or multiple regressions and nested models that predict BA by independent estimates of stem density and quadratic mean diameter. Direct multiple regression was the most accurate, giving a 9.6% Root Mean Squared Error of Prediction (RMSEP). The magnitude of the various errors introduced during the data collection stage is evaluated and their contribution to MSEP is analyzed. It was found that these errors accounted for less than 10% of model MSEP, suggesting that there is considerable scope for model improvement. Although site-specific models showed lower MSEP than global models, stratification by site may not be the optimal solution. The key to future improvement would appear to lie in a stratification that captures variations in relations between LiDAR and forest structure.

© 2012 Elsevier Inc. All rights reserved.

### 1. Introduction

Tropical forests offer a broad range of ecosystem services, from carbon sequestration to potential valuation of biodiversity components. But, forest conversion in the tropics has dramatically altered these services, and socio-demographic models predict that extensive tropical forest basins will undergo significant change in the coming decades (Wright, 2010). Although claims have long been made that these alterations will have an irreversible impact on ecosystem resilience and biodiversity conservation, it is only recently that studies have sought to quantify the real impact of these alterations on a global scale (Gibson et al., 2011). The international community is now aware of the serious consequences of tropical forest alteration on human welfare, partly thanks to issues connected with global climate change. A new round of international negotiations is being conducted under the UN Framework Convention on Climate Change (UNFCCC) with the aim of addressing a broad range of climate-related issues. One key focus is on developing policy-based incentives to mitigate forest degradation or clearing at the intergovernmental scale, and is called the REDD mechanism (Reducing Emissions by Deforestation

and Degradation). In its role as a framework for these negotiations, the Bali plan required a number of actions to be “measurable, reportable and verifiable”, and this prompted renewed interest in providing standardized and reproducible methods of forest structure measurement on a regional and global scale.

Of all the different monitoring procedures available, remotely sensed techniques have received the most attention for they potentially offer a detailed spatial description of forest status. Airborne- or satellite-borne light detection and ranging (LiDAR) has particular relevance in areas of high Above Ground Biomass (AGB > 250 Mg ha<sup>-1</sup>) where other remote sensing techniques, namely radar, provide only low resolution due to signal saturation (Le Toan et al., 2011). Efforts are also currently ongoing to combine radar and LiDAR data to improve the large-scale prediction of forest structure (Sun et al., 2011). LiDAR is an active remote sensing technology that measures distance by means of reflected laser light. In airborne laser scanning, the downward high-frequency emission of small footprint—typically sub meter—laser pulses from an airborne platform provides accurate data on the position of obstacles below, and a dense pattern of signal returns is obtained by the instrument's side-to-side sweep (scanning). Large airborne footprint (typically decameter) systems such as SLICER (Harding et al., 2001) and LVIS (Blair et al., 1999) are also used, as are space-borne systems such as GLAS (Zwally et al., 2002) that record a vertical profile of the returned laser energy from its footprint. Several

\* Corresponding author at: IRD AMAP CIRAD, TA A-51/PS2, 34398 Montpellier cedex 5, France. Tel.: +33 4 67 61 58 00x5283.

E-mail address: [gregoire.vincent@ird.fr](mailto:gregoire.vincent@ird.fr) (G. Vincent).

studies have demonstrated that LiDAR-derived metrics provide an accurate estimate of canopy forest structure (Asner et al., 2010; Hudak et al., 2009). However, the degree to which the relation between LiDAR metrics—that depend on sensor type—and forest structure varies across sites and forest types is poorly documented. For instance, Drake et al. (2003) showed that the relationship between a large footprint LiDAR-derived forest metric, the height of median energy (a proxy for mean canopy height), and AGB, differed between a seasonal moist forest in Panama and a wet forest in Costa Rica. Recently, Saatchi et al. (2011) produced a global AGB map of tropical forests based on a satellite-borne LiDAR instrument (Geoscience Laser Altimeter System, GLAS, onboard the Ice, Cloud, and land Elevation Satellite, acquired in 2003 and 2004). GLAS acquisitions were regressed with ground-based Lorey's height (basal area weighted height of all trees > 10 cm in diameter). Allometric relations between Lorey's height and AGB of calibration plots differed significantly in Central and South America, in Africa, and in South-East Asia. This further suggests that the relationship between LiDAR-derived metrics and forest characteristics are site-dependent.

Conversely, in their study that pioneered the application of large footprint full wave LiDAR (SLICER) in forest AGB predictions, Lefsky et al. (2002) concluded that the relationship between LiDAR metrics and AGB was stable across different biomes. In this they focused on three forest types: temperate deciduous, temperate coniferous and boreal forest. Their regression model used mean canopy height squared and the product of canopy cover and canopy height as predictors. Separate regressions by forest type did not significantly improve predictions. However, their conclusion may stem from the marked uncertainty of the predictions reported in their study and the limited statistical power of the analysis: the estimated residual error (digitized data from Fig. 2 in (Lefsky et al., 2002)) was about 70 Mg ha<sup>-1</sup> or 22%. This large residual error may be due to a combination of small plot size and limited precision of LiDAR footprint positions (Lefsky et al., 1999).

The scarcity of sites combining large-scale LiDAR coverage and extensive forest plot inventories over a broad range of forest types has slowed our efforts to evaluate the robustness and accuracy of small footprint airborne LiDAR predictions of closed-canopy tropical forest structure. In the study described herein, we address this issue by capitalizing on a large, ground-based forest inventory (129 ha total area) covering a great diversity of forest structures resulting from natural (soil and geological substrate) and anthropogenic effects (unlogged and logged forests), and full coverage of this site by a small footprint airborne LiDAR, in French Guiana, South Eastern America.

Non species specific pan tropical allometric equations linking tree AGB to tree height (h), stem diameter (d) at 1.3 m or above buttresses, and wood density, have been established for different forest types in different ecological zones (Chave et al., 2005). The explicit inclusion of tree height is essential to avoid bias associated with variations in the mean h–d relation across sites (Chave et al., 2005; Feldpausch et al., 2010; Vieilledent et al., 2011). A commonly used model of individual tree AGB has the following general form:

$$AGB = F * \rho * \left(\frac{\pi}{4} d^2\right) * h \quad (1)$$

where  $\rho$  is oven dried wood specific gravity, d is stem diameter in cm, h is total tree height in m and F is a form factor.

Stand volume equations based on a similar approach have long been used by foresters. The product of mean stand height, stand basal area and a stand form factor (capturing the average form factor for the stand) has been used to estimate stand cubic volume (Husch et al., 2002). LiDAR mainly provides information on vegetation height, either as top of canopy or as a vegetation profile, and foresters have devoted considerable effort to developing procedures that can be used to estimate stand height from LiDAR data (Næsset, 1997). Such

estimates are now considered to be robust (Hopkinson et al., 2006). On the other hand, the relation between stand height and stand basal area is expected to vary significantly between sites, even within ecological zones, reflecting variations in the h–d relation in individual trees (Chave et al., 2005). Hence, an assessment of site-to-site variability in LiDAR predictions of AGB must focus on the relation between LiDAR metrics and basal area (BA).

This focus on BA as a key variable when mapping AGB based on LiDAR data is further supported by the recent results of a multisite study (Asner et al., 2012) where a “universal” approach to predicting tropical forest biomass from LiDAR coverage was proposed and tested. By analogy with individual tree biomass models, the authors proposed to decompose plot level biomass as follows:

$$AGB_{\text{plot}} = aMCH^{b1} * BA^{b2} * WD_{BA}^{b3} \quad (2)$$

where BA is basal area in m<sup>2</sup>, WD<sub>BA</sub> is the basal area-weighted wood density of each plot, and MCH is Mean Canopy Height i.e. the vertical centre of the canopy volumetric profile (as opposed to simple top-of-canopy height). The initial results of this study, obtained by combining data from Panama, Hawaii, Madagascar and Peru, strongly suggest that local variability in the LiDAR-to-biomass relation can be efficiently captured by determining the site-specific relation between LiDAR metrics and BA, and assessing the wood density of local species. Conversely, Mean Canopy Height, as used in the above model, can be obtained unequivocally from LiDAR data in a site-independent manner on condition that standardized sensors and acquisition parameters are used across sites (Næsset, 2009). Here it is noteworthy that in the latter approach, the form factor—which relates stand height and BA to stand volume or biomass—is subsumed in the set of fixed parameters a, b1, b2 and b3 and is implicitly taken to be constant across sites.

The main aim of the study described herein was therefore to contribute to evaluating the robustness and accuracy of small footprint airborne LiDAR used to predict stand basal area (BA) and its components, quadratic mean diameter (Dg), and stand density (N), in undisturbed and logged over tropical moist forest. In particular, we were interested in (a) identifying the combination of LiDAR-derived canopy statistics that most accurately predicted the above-mentioned structural variables; (b) evaluating the accuracy of a general model adjusted to a large dataset encompassing different sites and different forest structures; (c) identifying the various sources of errors and assessing their contribution to overall uncertainty in a given regional context (French Guiana); (d) identifying areas of potential improvement for LiDAR predictions of BA (or AGB).

## 2. Material and methods

### 2.1. Study sites

A total of 129 one-ha square forest plots were selected at four different sites in French Guiana (Table 1, Fig. 1). The climate in French Guiana is equatorial with little variation in temperature and wind regime around the year (Boyé et al. 1979). Mean annual precipitation ranges from 1700 mm in the North–West to 3800 mm in the North–East (Cacao region). Seasonality is mostly related to the annual rainfall pattern, with lower precipitations around September and October. Climatic diagrams for two sites (PAR and NOU) located 135 km apart are provided as supplementary information (Fig. S1). Unlogged evergreen forest was the dominant vegetation sampled at all sites and totaled 89 plots. An additional 36 plots (PAR site) were logged experimentally at different intensities in 1984. Another four plots were set-up in forest regrowth (PSE site) in an area that was entirely clear-cut in 1976.

Stem diameter at all plots was recorded at 1.30 m or above basal irregularities such as buttresses for all trees with stem diameter

**Table 1**

Characteristics of the data collected for 129 one-ha forest plots in French Guiana. Site acronyms are explained in the **Material and methods** section.

Site	Year of ground inventory (area sampled)	Year of LiDAR scan	Mean number of pulses per m <sup>2</sup> (SD)	Comments
PAR	2009 (85 ha)	2009	12.4 (5.0)	Consolidated Canopy Height Model obtained by merging three scans taken over a 6-month period; 36 plots logged over.
MPB	2003 (10 ha) 2008 (6 ha) 2009 (1 ha)	2009	5.8 (3.1)	Highly contrasted forest structure, including a very large range of stem densities and canopy heights.
PSE—OldGrowth	2003 (11 ha)	2009	5.7 (2.6)	One 1000×100 m track+1 ha.
PSE—Spiro	2005 (1 ha) 2010 (1 ha)	2009	6.8 (3.4)	Low canopy forest dominated by a single species ( <i>Spirotropis longifolia</i> ).
PSE—ArboceI	2009 (4 ha)	2009	5.4 (2.3)	32-year-old secondary forest.
NOU—“Grand Plateau”	2008 (10 ha)	2007	4.5 (2.9)	One 1000×100 m track; very variable physiognomy.

greater than 10 cm. A botanical identification to genus or species was available for more than 80% of the trees in 124 plots.

The first study area consisted of the Paracou experimental research station (PAR, 85 plots, 5° 15' N, 52° 56' W). This was set up in the mid-1980s to provide baseline information on forest recovery after logging. The range of forest structure encountered here arises from natural variations in local drainage combined with different logging intensities (Gourlet-Fleury et al., 2004b; Vincent et al., 2010). The three logging treatments implemented in this area had reduced plot basal area by ca. 5, 10 and 15 m<sup>2</sup> ha<sup>-1</sup> from an initial average basal area of 31 m<sup>2</sup> ha<sup>-1</sup> (Gourlet-Fleury et al., 2004a). Our study considered 12 one-ha plots for each logging treatment.

The second study area was Piste de Saint-Elie (PSE, 17 plots, 5° 16' N, 53° 3' W) located 15 km west of Paracou. Four plots were set-up in secondary forest regrowth following complete clearing of the vegetation in 1976 (Sarrailh et al., 1990; Toriola et al., 1998). Two plots were selected in a patch of locally mono-dominant *Spirotropis longifolia* (Fonty et al., 2011), and the remaining 11 plots (one 1000×100 m plot, i.e. 10 contiguous 1-ha plots, plus one separate, square 1-ha plot) were selected in unlogged forest and were initially inventoried to study the relation between soil cover organization and floristic composition (Sabatier et al., 1997) before being re-censused in 2003 (Madelaine et al., 2007).

The third study area was Montagne Plomb (MPB, 17 plots, 5° 1' N, 52° 55' W), another important forest ecology research site in French Guiana. In all, 11 isolated one-ha plots and one 200×300 m plot were selected over a large area (~100 km<sup>2</sup>) and included a considerable diversity of forest structures. Forest structure in the area was shown by Paget (1999) to vary considerably in relation to soil

substrate and drainage regime. This floristic-soil relation was further studied by Sabatier et al. (2007) and high stem densities are found here on thin superficially drained soils (Couteron et al., 2005).

Finally, plot data from the Nouragues Ecological Research Station (NOU, 10 plots, 4°5' N, 52°41' W) were included in the study. Ground measurements at this site were taken from a 10-ha forest track (“Grand Plateau Bande L”, 1000×100 m) of very variable physiognomy: from high mature forest with fairly open understorey dominating in the northern part of the transect to low forest with locally abundant lianas dominating in the south (Chave et al., 2008; Poncy et al., 2001).

## 2.2. LiDAR data

All LiDAR coverage data were acquired in 2007 (NOU site) and 2009 (other sites) by a private contractor, Altoa (<http://www.altoa.fr/>), operating a helicopter-borne LiDAR. The helicopter flew between 120 and 220 m a.g.l. The system was composed of a scanning laser altimeter with a rotating mirror mechanism (Riegl LMS-Q140i-60 operated in 2007 and 2009, or newer LMS-280i operated in 2009), a GPS receiver (coupled to a second GPS receiver on the ground) and an inertial measurement unit to record the aircraft's pitch, roll and heading. Laser wavelength was 0.9 μm (near infrared), scanning angle was ±30° (LMS-Q140i-60) or ±15° (LMS-280i), and the laser recorded the last reflected pulse to within better than 0.1 m. The mean number of pulses per m<sup>2</sup> on a single acquisition was ~4, but this varied significantly across plots at any given site (Table 1). Mean footprint at ground level was about 45 cm (Riegl LMS-Q140i-60) or 10 cm in diameter (LMS-280i). The two systems were compared in 2009 at one site (PAR).

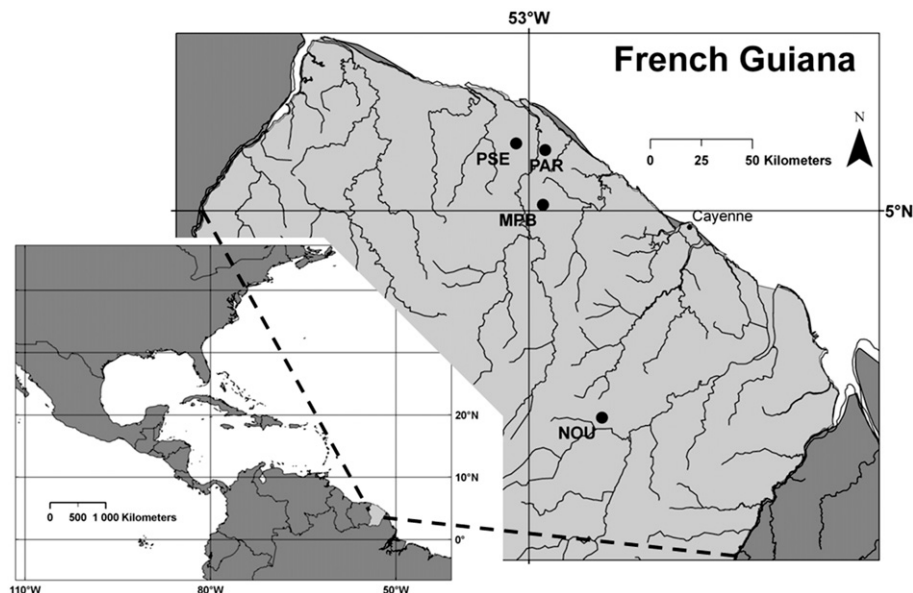


**Fig. 1.** Location map of the sites where the study was conducted.

Both systems had the capacity to record only a single return pulse. When conducting a preliminary test run with the LMS-Q 140i-60 at a density of 4 pulses  $m^{-2}$ , we found that recording the last return pulse increased the percentage of ground returns (which nevertheless remained typically below 1%). We also found that mean penetration (difference between first and last return) was  $\sim 2$  m, and that the mean Canopy Height Model (CHM) was 50 cm lower in last return mode than in first return mode.

Raw data points at each site were first processed to extract ground points using the TerraScan (TerraSolid, Helsinki) ground routine which classifies ground points by iteratively building a triangulated surface model. Ground points typically accounted for less than 1% of the total number of return pulses. A one-meter Canopy Surface Model was derived for each plot in our sample by considering the local maximum height on a  $1 \times 1$  m grid. Digital Terrain Model interpolated from the ground points was subtracted from the Canopy Surface Model to obtain the digital Canopy Height Model (CHM). A few cells—typically less than 2%—had no registered hits due to shading effects. In some cases a larger fraction of cells had no data due to the helicopter suffering strong pitch and roll locally in wind gusts, and this generated data gaps if the scans resulting from two successive flight lines failed to overlap. We did not use a filling algorithm to plug the few missing cells in the CHM; these were treated as missing data.

The CHM height distribution was used to generate statistics selected on the basis of previously attested performance in a similar context (Vincent et al., 2010): moment statistics (mean, standard deviation, skewness and kurtosis), order statistics (median, 10% and 90% percentiles) and the proportion of heights below 5 m (canopy gaps).

The height distribution for each of the 129 sample plots was further summarized using correspondence analysis (CA) applied to relative frequency in 13 five m-height bins (from 0 to 65 m). The coordinates on the first 3 axes were labeled CA1 to CA3 and together captured 83% of the total inertia (CA variance) of the height distributions in the 129 plots.

CA loadings efficiently capture differences between plot CHMs, and therefore assess the correlation between height distributions and stand variables. However, CA loadings have two disadvantages over more “objective” predictors. First, they may be difficult to relate to particular characteristics of the height distribution, and second, they are essentially dependent on the composition of the sample dataset.

Ground and LiDAR data were co-registered based on GPS geolocation. The standard procedure for geo-referencing plots was to acquire plot corner coordinates using a handheld GPS unit (Garmin CSX 60) with readings averaged over a 15-min period and acquire plot orientation (northing) with a hand-held compass. The plot was then positioned using GIS software based on the coordinates of its centre (average corner coordinates) and orientation. Overall precision for the X and Y coordinates of plot center was estimated from repeated corner measurements of 11 plots at the MPB site by different operators on different dates. Standard error on plot corner coordinates was found to be  $\sim 8$  m. The error on plot center coordinates was computed as the standard error of the mean of the four plot corners coordinates, i.e.  $\sim 4$  m. Plot geolocation was more precise at the PAR site as one corner per plot was geolocated using a differential GPS while the other three corners were positioned using a compass and a surveyor's rope. A 1 m error on plot center was considered to be a conservative estimate for all plots at this site.

### 2.3. Stand characteristics

The following were computed: basal area (BA in  $m^2 ha^{-1}$ , sum of the cross-sectional areas of all trees with  $d > 10$  cm per ha), quadratic mean diameter (Dg in cm, square root of the arithmetic mean square

diameter) and stem density (N per ha). Noting that (expressing Dg in m)

$$BA = N * Dg^2 * \frac{\pi}{4} \quad (3)$$

N and Dg can be viewed as elementary components of stand BA.

Log transforms of basal area components (Dg and N) were linearly correlated but this relation varied by site. Plots with extremely high stem densities at one site (MPB) showed a relatively large stem quadratic mean diameter (Fig. 2).

### 2.4. Models development

Different BA-predicting models were evaluated and compared. These comparisons involved simple (one predictor) regression vs. multiple (several predictors) regression models, site-specific vs. regional models, and nested vs. non-nested models.

Linear regression (glm procedure in R) was used to predict plot basal area (or its components) from a single predictor or a set of predictors selected from a set of LiDAR statistics using a step procedure and the minimum AIC selection criterion. To safeguard against possible over-fitting, we used leave-one-out cross-validation (cv.glm procedure in R boot package) and present RMSEP (Residual Mean Squared Error of Prediction) along with the global RMSE computed on the residuals of the model developed using the entire dataset. We also present the best single predictor model for each stand parameter.

As regional models do not distinguish between sites, site-specific models were built by adding a site factor (4 levels) to the most parsimonious multiple regression model. And regression coefficients were allowed to vary by site by including interactions between the site factor and the other factors included in the model.

Nested models were an alternative strategy used to directly regress plot BA with LiDAR metrics and consisting of separately regressing elementary components (N and Dg) then subsequently combining these components to compute BA. The rationale for testing such an approach is that the same BA can be achieved through various combinations of Dg and N and hence potentially different CHM characteristics (Fig. 2). Therefore, if LiDAR statistics correlate better with the elementary components of BA than with BA itself, it may prove more efficient to estimate these components separately. Additionally, as Dg is squared and multiplied by N to obtain BA, the error made on the elementary components may be amplified.

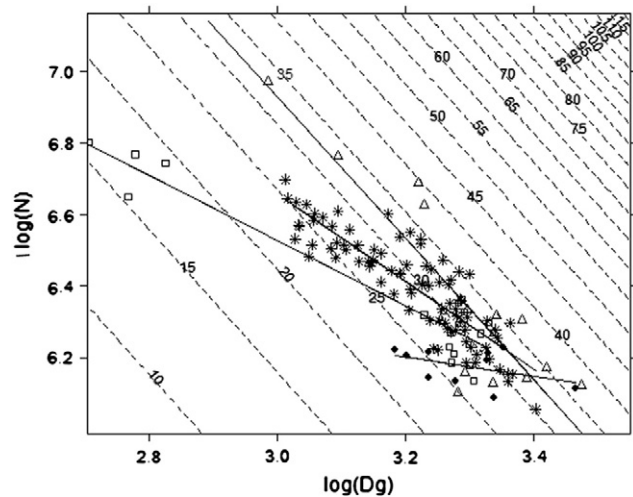


Fig. 2. Site variations in log transforms of quadratic mean diameter (Dg in cm) and stem density (N in stems  $ha^{-1}$ ); dotted lines represent basal area (BA in  $m^2 ha^{-1}$ ) iso-lines. Each point (observation) represents a 1-ha plot. Site coding: stars = PAR, open squares = PSE, open triangles = MPB, solid circles = NOU.

Simple regression (i.e. regression of a particular stand characteristic, namely BA, with a single statistic extracted from CHM) proved to be effective in a recent study (Asner et al., 2012) and has the merit of simplicity.

In our efforts to identify the best modeling strategies, we were particularly interested in comparing the performance of site-specific simple regression models with that of a multiple regression regional model of BA (taken as our reference model in the remainder of this manuscript). We also sought to assess the robustness of the nested models developed at site and regional levels.

Given the strong correlation ( $>0.99$ ) between mean, median and CA1, we omitted the last two variables in our initial set of explanatory variables, keeping only 10 candidate predictors: mean, standard deviation, skewness, kurtosis, 10% and 90% percentiles, maximum, proportion of heights below 5 m (inf5), CA2 and CA3.

## 2.5. Model error analysis

Various sources of error affecting the data may degrade model performance and need to be considered. Errors may affect the predictors extracted from the CHM or the values to be predicted which are themselves estimated from ground survey.

We successively evaluated the errors affecting the data used in model building and the impact of these errors on model predictions. We used Mean Square Error of Prediction (MSEP) as a measurement of model prediction accuracy, and estimated MSEP by cross validation (Leave-One-Out procedure). We refer the reader to Efron (1983) for a discussion of the properties of the commonly used cross-validation estimator relative to bootstrap estimators.

The formal decomposition of MSEP that we present below is borrowed from Wallach and Genard (1998).

Let  $y$  be the random variable to be predicted (i.e. the plot structural characteristic of interest BA, N or Dg) and let  $X$  be the random vector of the predictor variables (the vector of the statistics extracted from the CHM retained in the model). Since the predictors themselves carry some uncertainty, we do not have access to  $X$  itself but rather to estimated values  $\hat{X} = X + \varepsilon_x$ , where  $\varepsilon_x$  is the random error that is assumed to have zero expectation (predictors should be unbiased).

The prediction model is denoted  $f(\hat{p}, X)$ , where  $\hat{p}$  is the vector of the (estimated) model parameters. Since the parameters are estimated,  $\hat{p}$  is assumed to be a random vector and the conditional mean squared error of prediction of a model is defined as

$$MSEP(\hat{p}) = E \left\{ \left[ y - f(\hat{p}, \hat{X}) \right]^2 \right\} \quad (4)$$

The expectation is over all the random variables, i.e. over the individuals in the population (i.e. over plot values to be predicted) as well as over  $\hat{X}$  (i.e. the plot CHM statistics) and  $\hat{p}$  (the estimated parameters).

$MSEP(\hat{p})$  decomposes into (Wallach & Genard, 1998)

$$MSEP(\hat{p}) = \Lambda + \Delta + \Gamma \quad (5)$$

where

$$\Lambda = E[y - E(y|X)]^2 \quad (6)$$

$$\Delta = E \left[ E(y|X) - f(\hat{X}, \hat{p}|X) \right]^2 \quad (7)$$

$$\Gamma = E \left\{ \left[ E(f(\hat{X}, \hat{p}|X) - f(\hat{X}, \hat{p})) \right]^2 \right\} \quad (8)$$

$\Lambda$ , the “population variance”, represents the minimum  $MSEP(\hat{p})$  that can be achieved for a given choice of predictor variables, i.e. the irreducible random error in the model (Wallach & Genard, 1998). This term includes the error made on the plot variables to be predicted.

$\Delta$ , the “model bias”, measures the average squared difference between the average  $y$  for a given  $X$ , and the corresponding model prediction averaged over  $\hat{X}$  and  $\hat{p}$ .

$\Gamma$ , the “model variance”, represents the direct effect of uncertainty in the input variables (i.e. in the CHM statistics) or the model parameters.

We estimated the component of model variance due to uncertainty on the input variables by error propagation analysis after characterizing the error bearing on the CHM statistics. We also estimated the error bearing on the stand values to be predicted. The latter is introduced at the ground data collection stage and contributes to the population variance. The relative contribution of these errors to the MSEP of the different models was then assessed.

## 2.6. CHM statistics error analysis

The Mean Square Error of each of the CHM-derived predictors was evaluated by comparing replicate flights. Let  $x$  denote a particular CHM statistic (e.g. mean canopy height) and let  $\hat{x}$  be its estimator. The Mean Square Error of the estimator  $\hat{x}$  is defined as

$$MSE(\hat{x}) = E \left[ (\hat{x} - x)^2 \right] \quad (9)$$

where  $E$  is the expectation (over  $\hat{x}$ ), which can be re-written as (Tassi, 1989)

$$MSE(\hat{x}) = Var(\hat{x}) + (Bias(\hat{x}, x))^2 \quad (10)$$

This shows that MSE is the sum of the variance and the squared bias of the estimator.

The variance and bias of each statistic's estimator were estimated by using replicate flights over limited areas. By ANOVA, we decomposed the observed variance of each statistic into a plot effect, a scan effect (estimating bias of the statistic associated with a particular scan) and a residual variance (the variance of the estimator).

We also evaluated the contribution made by inaccurate plot location to the variance of each statistic. In this case no bias was expected. The variance of the estimator was assessed by one-way ANOVA using plots as unique predictor.

### 2.6.1. Error on CHM statistics

The various statistics extracted from the CHM were affected by sampling error and by the characteristics of the LiDAR system. Sampling error accrued due to the fact that the scanning procedure was essentially a sampling procedure: even at relatively high densities, only a fraction of the actual canopy was sampled and any particular location may have been sampled from a range of distances and from various viewing angles. Both these factors potentially affected the characteristics of return pulses. Furthermore, bias (systematic difference between scans) may have occurred since scan acquisition parameters such as height of flight above ground level, atmospheric conditions, and scanning density may all have varied to some extent between flights. And when different laser systems were used, laser system specifications (particularly detection threshold, emitted pulse energy, and also in the present case swath angle) may produce systematic difference between scans (Næsset, 2009).

Sampling error in LiDAR acquisition (identical acquisition parameters). We first evaluated the repeatability of independent acquisitions made on a given day and using identical LiDAR settings (Riegl LMS-Q140i-60, 45 cm footprint,  $\pm 30^\circ$  scanning angle). We used four replicate acquisitions over a 30-ha block at the MPB site but along different flight lines. The acquisition characteristics for each LiDAR scan were similar: mean pulse density per  $m^2$  was 4.3 with a standard deviation of 2.5 including 4% missing cells.

LiDAR sensitivity to distinct acquisition parameters. Working on a 25-ha block of the PAR site, we compared the difference between two

acquisitions made 6 months apart (April and October) using different parameters: Riegl LMS-Q140i-60 (larger footprint and swath angle) and LMS-280i (smaller footprint and swath angle). Mean pulse density per m<sup>2</sup> was 5.3 (sd = 2.6; 1.9% missing cells) in the April scan and 5.2 (sd = 2.6; 2.4% missing cells) in the October scan.

**Error in plot location.** We randomly shifted plot boundaries without any deformation. Shifts in X and Y coordinates were sampled independently from a normal distribution with mean = 0 and standard deviation = 4 m for plots outside the PAR site and mean = 0 and standard deviation = 1 m for plots within the PAR site. We recomputed plot-related LiDAR statistics based on the new locations, and repeated the process 50 times.

### 2.6.2. Uncertainty propagation

Two 10-dimensional distributions of error affecting the 10-dimensional vector of predictors resulting (1) from LiDAR acquisition error and (2) from plot location error were generated. Once the error bearing on CHM-derived statistics had been characterized, we computed error propagation by modeling the process in a digital simulation, as follows. For every plot we re-sampled both the distribution of errors, added these terms to the observed values of CHM statistics, and applied the various stand parameters-predicting models to the noisy dataset (i.e. the original CHM statistic to which the error term was added). Note that the error term applied to the CHM statistics for each observation (each 1-ha plot) was selected independently but conserved the correlation structure of the error vector between the different CHM statistics. The same procedure was used for single predictor models, multiple regression models and the nested model. We ran 1000 such simulations and report error mean.

### 2.6.3. Error affecting the values to be predicted

**Error in plot area.** Measurements of plot area are prone to error, especially in rugged terrain where sloping is uneven. We estimated plot area error by running simulations and considered an error of 2 m for plot side and one degree for plot side azimuth (assuming these errors to be independent).

**Temporal lag between LiDAR acquisition and ground inventories.** Some plots in our sample (11 plots in PSE, and 10 plots in MPB) had been surveyed 5 to 6 years before the LiDAR scan was acquired, and there was some time lag for many plots between the ground survey and the LiDAR scan (see Table 1). This time lag contributed to the model's overall prediction error as it created uncertainty on actual plot BA on the day of the LiDAR scan. We used data from old growth, unlogged forest at the PAR experimental site (where regular inventories had been conducted every other year) to assess the magnitude of this source of error. We were therefore able to estimate the error arising from 2, 4 and 6 years of discrepancy between laser scan and field inventory dates.

To facilitate comparisons of the magnitude of the error affecting various structural variables, we computed the relative Root Mean Squared Error (rRMSE) as the ratio of the RMSE to the prediction mean:

$$\text{Relative RMSE} = \sqrt{\frac{\sum_{i=1}^n \epsilon_i^2}{n-p}} * \frac{1}{\frac{1}{n} \sum_{i=1}^n \hat{y}_i} \quad (11)$$

where n is the total number of obs,  $\hat{y}_i$  is the predicted value for observation i,  $\epsilon_i$  is the error term  $\epsilon_i = y_i - \hat{y}_i$ , and p is the number of parameters used in the model.

## 3. Results

### 3.1. Most accurate predictive models

The magnitude of the error varied between stand variables (Table 2, Fig. 3). Stem density had the highest RMSE and Dg the lowest, while the RMSE for BA predictions was intermediate. Regressing

BA with LiDAR metrics yielded slightly better predictions (lower RMSE and higher r<sup>2</sup>) than the nested procedure where components were estimated separately and BA was computed subsequently (compare M2 and M4 in Table 2).

The most accurate multiple regression models systematically retained some CA loadings (last column in Table 2). Multiple regression models yielded more accurate predictions (lower RMSEP) than single regression models, and this applied for site-independent models (M2 vs. M5, M8 vs. M10, M12 vs. M13), site-specific models (M1 vs. M3) and nested models (M4 vs. M7).

Site-specific models (Fig. 3d) were systematically more accurate (lower RMSEP) than their site non-specific counterpart (for all stand variables predicted and model structures used, Fig. 3c and d illustrate the case for BA). However, an increase in the difference between RMSEP and RMSE indicated some degree of over-fitting when applying multiple regression per site of BA (M1 in Table 2).

Models using site and a single CHM statistic as predictors performed on a par with the non site specific multiple regression of CHM statistics when predicting BA (M2 and M3 in Table 2), fared less well when predicting Dg (M8 and M9) and significantly better when predicting stem density (M11 and M12).

### 3.2. Error analysis

**Error bearing on the predictors.** The error associated with LiDAR scan repeatability, sensitivity to LiDAR acquisition parameters and plot location uncertainty, and bearing on the various statistics extracted from the CHM, is reported in Table 3.

Some CHM-derived statistics appeared to be significantly biased (Table 3). However, the contribution made by the squared bias to MSE in LiDAR-derived statistics was generally far smaller than the variance of the estimator, and systematically less than 1% of the total variance. Therefore, in the remaining—and notably in the uncertainty analysis—we neglected bias and treated the global error bearing on the predictors as white noise.

Some statistics appeared to be less stable than others. For instance, the frequency of heights below 5 m (inf5) showed the highest Mean Squared Error (MSE). Similarly, the MSE of dec1 was typically 4- or 5-fold the MSE of dec9 as a result of a lower sampling intensity of lower areas in the CHM (interstitial spaces between crowns).

The plot location uncertainty in Table 3 was as expected under standard field conditions (i.e. it does not apply to the PAR site where plot location was more precise through differential GPS positioning of plot corners). Under standard conditions this plot location uncertainty tended to induce less error on the LiDAR statistics (lower MSE) than did LiDAR acquisition uncertainty. However, LiDAR type and settings had only a moderate impact on LiDAR statistics on the 1-ha scale, and this impact was similar in magnitude to the noise observed between independent acquisitions using the same settings.

Table 4 (column 4) shows the propagated error on the various stand variable predictions for the set of models presented in Table 2.

#### 3.2.1. Error on predicted plot variables

In addition to the uncertainty carried by the predictors, uncertainty regarding true plot area and time lag between field inventory and LiDAR acquisition also needed to be considered as this contributes directly to overall model error.

**Plot area.** The simulation procedure described in the Material and method section gave a mean plot area error of 2.7% which translated into a similar error on basal area.

**Time lag between acquisitions.** Error on BA estimates accruing from using 6-year-old inventory data was of the order of 3% (Fig. 4) and affected about 20% of the sample. A time lag of 2 years induced a BA error of ~1.3%. We evaluated the overall time lag contribution for all the plots by weighting the error committed for a particular

**Table 2**

Summary statistics of multiple and single linear regressions of forest stand structure variables from LiDAR-derived canopy height variables in 129 one-ha plots in French Guiana. BA = basal area in m<sup>2</sup>, Dg = quadratic mean diameter in cm, N = stand density in stems per ha. Predictors are extracted from the heights distribution in the LiDAR-derived Canopy Height Model: mean, standard deviation (sd), skewness (skew), kurtosis (kurt), 90% percentile (dec9), coordinates on axes 2 (CA2) and 3 (CA3) of a correspondence analysis on height frequency distribution. Site is a site factor as in Table 1. Predictors were selected on minimum AIC criterion. RMSEP is the Root Mean Square Error on Prediction, RMSE is the Root Mean Square Error of the model, rRMSE is the relative RMSE.

	Dependent variable	Model	R2	adj.R <sup>2</sup>	RMSEP	RMSE	rRMSE	df	Predictors
M1	BA	Multiple regression per site	0.73	0.68	2.72	2.31	7.9%	105	sd dec9 skew CA2 CA3 Site
M2	BA	Multiple regression	0.56	0.54	2.80	2.76	9.5%	124	sd dec9 skew CA2 CA3
M3	BA	Single regression per site	0.56	0.54	2.88	2.77	9.5%	121	mean Site
M4	BA	Nested multiple regression	0.53	0.49	3.02	2.9	9.9%	118	sd kurt mean CA2 skew CA3
M5	BA	Simple regression	0.42	0.41	3.15	3.11	10.7%	127	mean
M6	BA	Nested simple regression per site	0.49	0.42	3.28	3.28	11.2%	113	mean Site dec9
M7	BA	Nested simple regression	0.37	0.36	3.35	3.35	11.4%	125	mean dec9
M8	Dg	Multiple regression	0.85	0.84	1.24	1.22	4.9%	124	sd kurt mean CA2
M9	Dg	Simple regression per site	0.83	0.82	1.37	1.31	5.2%	121	mean Site
M10	Dg	Simple regression	0.75	0.75	1.57	1.56	6.2%	127	mean
M11	N	Simple regression per site	0.83	0.82	59.7	54.6	9.1%	121	dec9 Site
M12	N	Multiple regression	0.65	0.64	79.8	76.9	12.8%	123	sd skew kurt mean CA3
M13	N	Simple regression	0.59	0.59	83.4	82.1	13.6%	127	dec9

time lag by the corresponding number of plots. This yielded an estimated 0.3% error for Dg, 0.5% for stem density and 0.8% for BA.

By subtracting the contribution of these error components to  $\widehat{MSEP}$  (the estimated MSEP) we estimated the “intrinsic” model error i.e. the MSEP that would be achieved should these errors be 0 (Table 4). For all the models tested, the errors affecting the data used in model building which contributed either to the model variance or to the population variance (as defined in Section 3.2), made up less than 13% of  $\widehat{MSEP}$  (Table 4), indicating that the error in model predictions was predominantly due to intrinsic model shortcomings.

Finally, we computed local bias as the mean of predicted values minus observed values per site and per forest type, and this for each stand variable and the different regional multiple regression models used (Table 5).

With the exception of monodominant *Spirotropis* forests, the different forest types did not show severe bias. *Spirotropis* forest plots were subject to marked overestimation of stem density and marked underestimation of plot quadratic mean square diameter. These biases of opposite sign partly offset each other in the nested BA prediction model (line 1 in Table 5 and Fig. 3, plots SPM and SPQ).

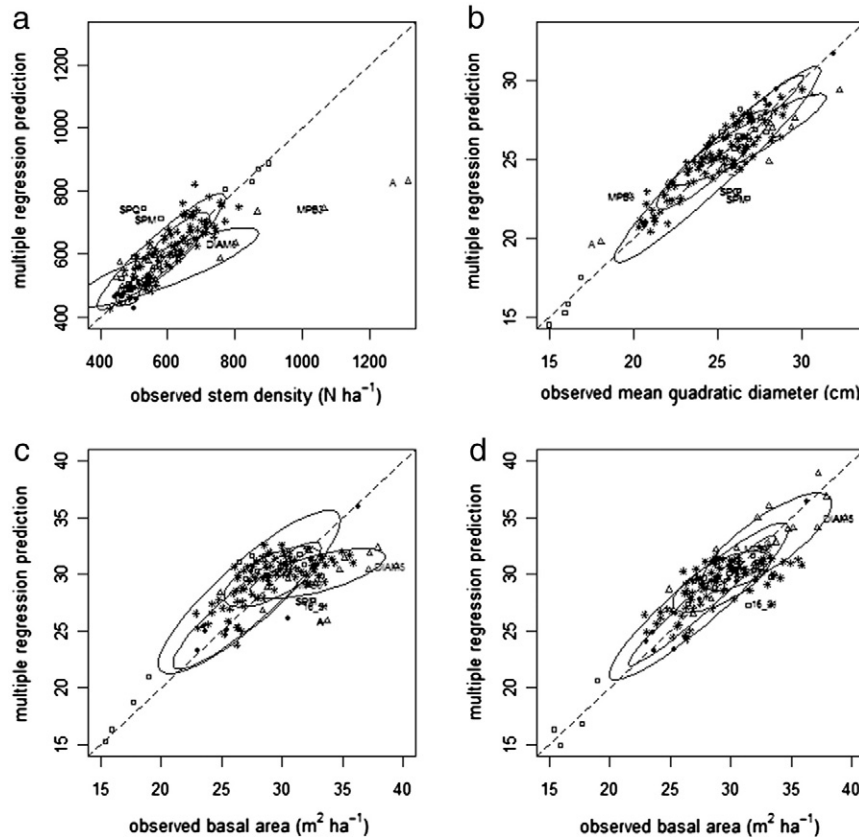


**Fig. 3.** Scatterplot of observed values vs. multiple regression prediction of (a) N (stem density); (b) Dg (quadratic mean stem diameter); (c) BA (basal area); (d) BA (basal area) regression adjusted by site. A few outlier plots (A, MPB3, DIAM5, SPM, SPQ, 16\_21) are discussed in the text. Confidence Gaussian bivariate ellipse drawn for P=0.67; Site coding: stars = PAR, open squares = PSE, open triangles = MPB, solid circles = NOU.

**Table 3**  
Mean Square Error bearing on statistics derived from the Canopy Height Model (% of total variance); MSE is the sum of squared bias and variance of the estimator (see Eq. 5 in text); significance of the bias (P value for Fisher's exact test in ANOVA): \*\* corresponds to  $P < 0.01$ , \* corresponds to  $P < 0.05$ , – corresponds to  $P > 0.05$ .

Statistic	LiDAR scan repeatability (30 ha × 4 replicates; MPB site)		LiDAR scan sensitivity to swath angle and footprint size (25 ha × 2 replicates; PAR site)		Plot location uncertainty (SE = 5 m, 40 ha × 50 replicates; MPB, PSE, NOU sites)
	MSE	Squared bias	MSE	Squared bias	MSE (no bias)
mean	2.70%	0.38% **	0.74%	–	0.38%
sd	1.93%	–	1.75%	0.73%**	0.39%
dec1	5.44%	0.47%**	1.30%	0.31%*	1.77%
dec9	0.75%	0.12%**	0.25%	0.06%*	0.33%
inf5	5.05%	–	2.83%	–	2.18%
CA2	3.35%	–	0.57%	–	0.69%
CA3	3.32%	–	1.54%	–	1.49%
kurt	3.30%	–	1.71%	–	1.56%
skew	1.95%	–	1.42%	0.54%**	0.98%

We found that all variables at the MPB site were consistently underestimated by all regional models used (see also Fig. 3).

#### 4. Discussion

Our regional (site-independent) model of BA carries an RMSEP of  $2.8 \text{ m}^2 \text{ ha}^{-1}$  (9.6%). A small (<10%) albeit significant part of the Mean Squared Error of Prediction can be traced back to the data collection procedure and is not strictly inherent to the model. Therefore, most of the MSEP must be ascribed to the model itself. Site-to-site variations in the relations between LiDAR metrics and stand variables probably contribute to this MSEP, as indicated by the fact that the RMSEP decreased when the models were adjusted by site (Table 2). However, when a site factor was included, this did not substantially reduce MSEP (for instance, compare M1 and M2 in Table 2). The MSEP likely stemmed from within site variations in the relations between LiDAR statistics and stand variables (see for instance Table 5 Logged-over forest (LOF), or *Spirotropis* dominated forest (MF)). This is further supported by the fact that models which included site-specific regressions (Fig. 2d) did not remove all pre-identified outliers. For instance, BA in plot “16–21” at the PAR site was still poorly predicted. This plot is dominated by swamp forest that has its own peculiar structure composed of abundant small palm trees (*Euterpe oleracea*) and a few large emergent trees. Plot “Diam5” at the MPB site is highly stocked (Fig. 3a) and was an outlier in the regression by site (Fig. 3d), while two other strong outliers (A and MPB3) fell back in line with predictions once the site was included in the model.

Miscellaneous potential sources of error in the model were considered. Systematic error in predictors (i.e. bias) may have contributed to the MSEP reported here. Two such sources of bias (difference in acquisition parameters either between replicate flights or between different LiDAR systems) were evaluated and considered negligible (Table 4). Swath angle was in principle of concern as larger angles increase shading effects and therefore increase the proportion of undetected lower points such as interstitial gaps between crowns. Excluding the lowermost points would affect all the LiDAR statistics considered here. The size of the laser foot print might also affect the likelihood of the laser beam being intercepted by canopy elements, and hence affect the CHM. These effects, however, seemed to be negligible compared to overall sampling noise on the 1-ha scale of the summary statistics (see results in Section 3.3) and in this study were included in the variance of the predictors' estimators. DTM extraction quality, on which CHM quality depends, may be of greater significance. DTM quality is likely to depend on terrain regularity, vegetation density and LiDAR pulse density, which together also affect the output of the procedure used to retrieve ground points (Clark et al., 2004; Xiaoye Liu, 2008). However, this is liable to become a stringent issue only in cases of extremely rugged terrain and/or low scanning density, and probably contributed little to the prediction error observed in the present study. Ground-surveyed topographic data were available at one site (PAR) to validate DTM, which was found to be acceptable (mean difference = 0.02 m, SD = 0.57,  $n = 730$ ). More significant sources of bias in this study consisted of idiosyncratic differences between forest types in the relation between canopy statistics and forest structure. These biases can locally

**Table 4**  
Contribution of various sources of error to MSEP in models predicting stand variables (BA = basal area in  $\text{m}^2$ , Dg = quadratic mean diameter in cm, N = stand density in stems per ha) from statistics derived from the Canopy Height Model. Errors affecting predicted stand variables arise from inaccurate plot measurement or a time lag between plot inventory and LiDAR scan. Errors affecting LiDAR statistics arise from the combined effects of inaccurate plot location and noise in the LiDAR signal.

Source of error							
Model	Dependent variable	Model	CHM statistics	Plot size	Time lag	RMSEP	Sampling error contribution to MSEP <sup>a</sup>
M1	BA	Mul. reg. per site	0.52	0.79	0.23	2.72	13%
M2	BA	Multiple regression	0.29	0.79	0.23	2.8	10%
M3	BA	Simple reg. Per site	0.23	0.79	0.23	2.88	9%
M4	BA	Nested mul. regression	0.28	0.79	0.23	3.02	8%
M5	BA	Simple regression	0.26	0.79	0.23	3.15	8%
M6	BA	Nested sim. reg. per site	0.52	0.79	0.23	3.28	9%
M7	BA	Nested sim. regression	0.42	0.79	0.23	3.35	8%
M8	Dg	Multiple regression	0.16	–	0.08	1.24	2%
M9	Dg	Sim. reg. per site	0.28	–	0.08	1.37	5%
M10	Dg	Simple regression	0.26	–	0.08	1.57	3%
M11	Dens	Sim. reg. per site	9	16	3	59.7	10%
M12	Dens	Multiple regression	6	16	3	79.8	5%
M13	Dens	Simple regression	6	16	3	83.4	4%

<sup>a</sup>  $[(\text{Error\_CHM})^2 + (\text{Error\_Plot\_Size})^2 + (\text{Error\_Time\_lag})^2] / (\text{RMSEP})^2$ .



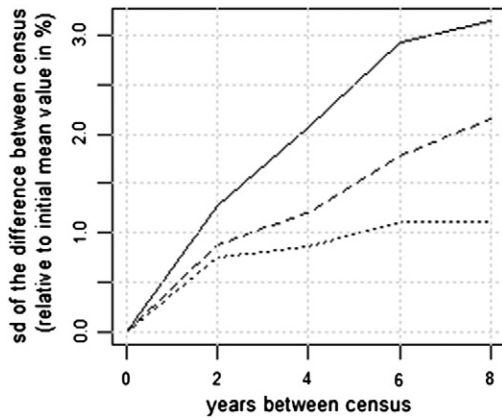


Fig. 4. Effect of time lag between successive inventories on change in stand parameters evaluated for 24 one-ha plots of undisturbed forest (Paracou 1999–2007); solid line: BA, dashed line: stem density, dotted line: Dg.

be substantial, as suggested by the apparent specificity of the MPB site (Table 5). Here, BA was consistently underestimated by a regional model, and a nested model did not improve prediction accuracy.

Similarly, BA components of *Spirotropis*-dominated plots (SPM and SPQ, Fig. 3a and b) were poorly estimated, with density being overestimated and Dg underestimated. Unsurprisingly, BA was also poorly estimated (Fig. 3c).

The above observations suggest that a hierarchical approach may prove more efficient for predicting biomass than an elusive one-size-fits-all relation between LiDAR statistics and forest structure parameters. Prior stratification by age class and site quality has been advocated for boreal forest (Næsset, 2002). In the present case, a site-adjusted model improved  $r^2$  substantially (Table 2, compare l. 1 and 2, and Fig. 3d), but suffered from over-parameterization.

How did our regional (site-independent) model compare with previously published models? As mentioned earlier, Lefsky et al. (2002) achieved fairly low precision using large-footprint LiDAR to study boreal and temperate forest structure. Drake et al. (2002) also used a large-footprint airborne LiDAR for their study of tropical forest canopy at the La Selva Biological station in Costa Rica. They obtained a plot level RMSE of 3 m<sup>2</sup> for basal area and 2 cm for Dg, i.e. slightly larger than those reported for our site-independent model (Table 2). No data were given in their paper for stem density predictions. Their results were based on heterogeneous field dataset sources and plot sizes (plots ranged in size from 0.05 to 0.5 ha) and included non-forest land (pasture). Hall et al. (2005) studying Ponderosa pine forest structure using small footprint LiDAR obtained an RMSE of ca. 5.8 m<sup>2</sup> (ca. 20%) for BA (n = 41) and 158 stems ha<sup>-1</sup> (ca. 44%) for N. No data were provided for Dg. Average plot size in their study was 0.28 ha (ranging from 0.16 to 0.75 ha).

A series of more recent studies (Asner et al., 2010; Asner et al., 2012; Mascaro et al., 2011) estimated biomass on the 1-ha scale with precision of ~10%, i.e. similar to that found here for BA in our regional model.

Asner et al. (2012) argue that Mean Canopy Profile Height should be used rather than mean CHM as this has been shown to provide a

“slight but consistent improvement”. This may indeed be the case but could not be evaluated here since the LiDAR system employed recorded only a single return pulse with low penetration and resulted in a shallow canopy profile. However, since the extent of laser beam penetration is determined by a complex interaction between the laser signal and the characteristics of the vegetation (Chasmer et al., 2006; Hopkinson, 2007) it may also be the case that mean top of canopy height is a more robust predictor than mean canopy profile height. This may notably become an issue in comparative studies where systems and acquisition parameters are likely to differ. As discussed above, CHM statistics are not insensitive to variations in acquisition parameters, but may nevertheless be more stable than statistics extracted from canopy profile. We suggest that, whenever possible, both approaches should be followed through at this stage.

Our regional multiple regression model therefore compares well with previously published studies conducted in tropical forest using either large footprint full wave (Drake et al., 2002) or small footprint discrete return LiDAR (Asner et al., 2010). This may partly be due to larger field plots than in previous studies and which tended to reduce the noise on predicted surface-based forest structure parameters (Frazer et al., 2011). Increasing plot size also reduces the border-to-surface ratio (and thereby reduces the weight of borderline individuals) and increases border length, thereby decreasing the likelihood of strong omission/commission imbalances. (Mascaro et al., 2011) using the 50-ha forest dynamics plot in Barro Colorado Island found in particular that this border effect became negligible for plots of about 1 ha.

Stratification into homogeneous forest types is likely to increase model precision for AGB even more significantly than for the other stand parameters considered here since stratification by site or forest type is expected to reduce the dispersion in h-d relations and the dispersion in plot mean wood density. For instance, we found that 29% of the variance in plot mean wood density could be attributed to the site, after excluding extreme values from secondary forest, *Spirotropis*-dominated forest and four plots where no taxonomic information was available. This supports a previous observation that regional scale variations in plot mean wood density are very marked in the Amazon basin (Baker et al., 2004).

## 5. Conclusion

Plot AGB estimates derived from field measurements can be severely biased if individual tree biomass is estimated without considering tree height. This bias is due to spatial variations in plot average h-d relations. In the study described herein, we therefore focused on predicting BA and its components (stand density and mean quadratic diameter Dg), rather than AGB.

Our results support earlier independent work that highlighted the great potential of LiDAR for remote sensing tropical forest structure parameters. Regional linear models of single or multiple canopy LiDAR metrics are applicable across sites and forest types and provide estimates of BA (or its components) or AGB with reasonable accuracy (relative RMSEP less than 10% for BA). Models based on a single regression per site performed almost on a par with multiple regression, non-site specific models. Multiple regression site-specific models

Table 5

Mean prediction error per site and per forest type in stand structure variables: basal area (BA), Quadratic mean diameter (Dg) and stand density (dens); Forest type coded as PF = unlogged old growth forest, LOF = Logged-over forest, MF = *Spirotropis* monodominant forest, SF = 32-year-old secondary forest.

Variable	Group (plot number n)	PF (n = 87)	LOF (n = 36)	MF (n = 2)	SF (n = 4)	MPB (n = 17)	NOU (n = 10)	PAR (n = 85)	PSE (n = 17)
BA	Nested model (M4)	1.0%	−4.4%	3.1%	1.9%	8.9%	−1.2%	−2.0%	−2.3%
	Mul. reg. (M2)	0.9%	−2.7%	6.1%	−4.0%	9.1%	−0.7%	−1.4%	−3.1%
Dens	Mul. reg. (M8)	1.4%	−1.4%	−31.7%	−0.2%	9.5%	2.2%	−1.0%	−5.9%
		0.2%	−1.5%	14.2%	1.2%	2.0%	−1.8%	−0.6%	1.9%

were significantly more precise but tended to lack prediction robustness given the associated reduction in calibration data available per site.

Less than 10% of the Mean Squared Error of Prediction in the regional site-independent model is likely to stem from error affecting data collection. This suggests that there is considerable scope for improving model accuracy. A large proportion of the prediction error is believed to originate from idiosyncratic differences between forest types in the way LiDAR statistics relate to forest structural variables. The error due to the heterogeneity of forest types could be reduced by first stratifying the forest into homogeneous types (with respect to the LiDAR-to-forest structure relationship) and adjusting specific models per stratum. It remains to be ascertained whether the segmentation of forest types from LiDAR data (and possibly other type of remotely sensed data) could be used to efficiently identify these homogeneous types and by how much error could be reduced. Another—non-exclusive—strategy would be to improve stem density estimates which are far less accurate than quadratic mean diameter estimates (Table 2). This seems worth exploring since the nested approach to BA prediction performed almost as well in our study as the direct regression approach. Both paths (stratification and improvement in stem density estimation) may benefit from extracting texture indices from CHM instead of simple frequency-based statistics as were used here.

## Acknowledgments

This study was partially funded by the European Regional Development Fund (ERDF contract no. 2907 dated 04/11/08). We wish to thank two anonymous reviewers whose comments helped to improve the manuscript significantly and Mark Jones (TransCriptum) for revising the English. This is a publication of Laboratoire d'Excellence CEBA (ANR-10-LABX-25).

## Appendix A. Supplementary data

Supplementary data to this article can be found online at <http://dx.doi.org/10.1016/j.rse.2012.06.019>.

## References

- Asner, G. P., Mascaro, J., Muller-Landau, H. C., Vieilledent, G., Vaudry, R., Rasamoelina, M., et al. (2012). A universal airborne LiDAR approach for tropical forest carbon mapping. *Oecologia*, 168, 1147–1160.
- Asner, G. P., Powell, G. V. N., Mascaro, J., Knapp, D. E., Clark, J. K., Jacobson, J., et al. (2010). High-resolution forest carbon stocks and emissions in the Amazon. *Proceedings of the National Academy of Sciences*, 107, 16738–16742.
- Baker, T. R., Phillips, O. L., Malhi, Y., Almeida, S., Arroyo, L., Di Fiore, A., et al. (2004). Variation in wood density determines spatial patterns in Amazonian forest biomass. *Global Change Biology*, 10, 545–562.
- Blair, J. B., Rabine, D. L., & Hofton, M. A. (1999). The Laser Vegetation Imaging Sensor (LVIS): A medium-altitude, digitization-only, airborne laser altimeter for mapping vegetation and topography. *ISPRS Journal of Photogrammetry & Remote Sensing*, 56, 112–122.
- Boyé, M., Cabaussel, G., & Perrot, Y. (1979). *Atlas des départements français d'Outre-Mer: 4. La Guyane*. Bordeaux-Talence & Paris: CEGET, Centre d'études de géographie tropicale du CNRS & ORSTOM, Office de la recherche scientifique et technique outre mer.
- Chasmer, L., Hopkinson, C., Smith, B., & Treitz, P. (2006). Examining the influence of changing laser pulse repetition frequencies on conifer forest canopy returns. *Photogrammetric Engineering & Remote Sensing*, 72, 1359–1367.
- Chave, J., Andalo, C., Brown, S., Cairns, M. A., Chambers, J. Q., Eamus, D., et al. (2005). Tree allometry and improved estimation of carbon stocks and balance in tropical forests. *Oecologia*, 145, 87–99.
- Chave, J., Olivier, J., Bongers, F., Châtelet, P., Forget, P.-M., van der Meer, P., et al. (2008). Above-ground biomass and productivity in a rain forest of eastern South America. *Journal of Tropical Ecology*, 24, 355–366.
- Clark, M. L., Clark, D. B., & Roberts, D. A. (2004). Small-footprint lidar estimation of sub-canopy elevation and tree height in a tropical rain forest landscape. *Remote Sensing of Environment*, 91, 68–89.
- Couteron, P., Pelissier, R., Nicolini, E. A., & Paget, D. (2005). Predicting tropical forest stand structure parameters from Fourier transform of very high-resolution remotely sensed canopy images. *Journal of Applied Ecology*, 42, 1121–1128.
- Drake, J. B., Dubayah, R. O., Knox, R. G., Clark, D. B., & Blair, J. B. (2002). Sensitivity of large-footprint lidar to canopy structure and biomass in a neotropical rainforest. *Remote Sensing of Environment*, 81, 378–392.
- Drake, J. B., Knox, R. G., Dubayah, R. O., Clark, D. B., Condit, R., Blair, J. B., et al. (2003). Above-ground biomass estimation in closed canopy Neotropical forests using lidar remote sensing: Factors affecting the generality of relationships. *Global Ecology & Biogeography*, 12, 147–159.
- Efron, B. (1983). Estimating the error rate of a prediction rule: Improvement on cross-validation. *Journal of the American Statistical Association*, 78, 316–331.
- Feldpausch, T. R., Banin, L., Phillips, O. L., Baker, T. R., Lewis, S. L., Quesada, C. A., et al. (2010). Height-diameter allometry of tropical forest trees. *Biogeosciences Discuss*, 7, 7727–7793.
- Fonzy, É., Molino, J.-F., Prévost, M.-F., & Sabatier, D. (2011). A new case of neotropical monodominant forest: *Spirotropis longifolia* (Leguminosae–Papilionoideae) in French Guiana. *Journal of Tropical Ecology*, 27, 641–644.
- Frazier, G. W., Magnussen, S., Wulder, M. A., & Niemann, K. O. (2011). Simulated impact of sample plot size and co-registration error on the accuracy and uncertainty of LiDAR-derived estimates of forest stand biomass. *Remote Sensing of Environment*, 115, 636–649.
- Gibson, L., Lee, T. M., Koh, L. P., Brook, B. W., Gardner, T. A., Barlow, J., et al. (2011). Primary forests are irreplaceable for sustaining tropical biodiversity. *Nature*, 478, 378–381.
- Gourlet-Fleury, S., Favrichon, V., Schmitt, L., & Petronelli, P. (2004a). Consequences of silvicultural treatments on stand dynamics at Paracou. *Ecology and management of a neotropical rainforest: Lessons drawn from Paracou, a long-term experimental research site in French Guiana* (pp. 254–280). Paris: Elsevier.
- Gourlet-Fleury, S., Guehl, J.-M., & Laroussinie, O. (2004b). *Ecology and management of a neotropical rainforest: Lessons drawn from Paracou, a long-term experimental research site in French Guiana*. Paris: Elsevier.
- Hall, S. A., Burke, I. C., Box, D. O., Kaufmann, M. R., & Stoker, J. M. (2005). Estimating stand structure using discrete-return lidar: An example from low density, fire prone ponderosa pine forests. *Forest Ecology and Management*.
- Harding, D. J., Lefsky, M. A., Parker, G. G., & Blair, J. B. (2001). Laser altimeter canopy height profiles: Methods and validation for closed-canopy, broadleaf forests. *Remote Sensing of Environment*, 76, 283–297.
- Hopkinson, C. (2007). The influence of flying altitude, beam divergence, and pulse repetition frequency on laser pulse return intensity and canopy frequency distribution. *Canadian Journal of Remote Sensing*, 33, 312–324.
- Hopkinson, C., Chasmer, L., Lim, K., Treitz, P., & Creed, I. (2006). Towards a universal lidar canopy height indicator. *Canadian Journal of Remote Sensing*, 32, 139–152.
- Hudak, A. T., Evans, J. S., & Smith, A. M. S. (2009). LiDAR utility for natural resource managers. *Remote Sens.*, 1, 934–951.
- Husch, B., Beers, T. W., & Kershaw, J. A. (2002). *Forest mensuration*. : John Wiley & Sons.
- Le Toan, T., Quegan, S., Davidson, M. W. J., Balzter, H., Paillou, P., Papatthanassiou, K., et al. (2011). The BIOMASS mission: Mapping global forest biomass to better understand the terrestrial carbon cycle. *Remote Sensing of Environment*, 115, 2850–2860.
- Lefsky, M. A., Cohen, W. B., Harding, D. J., Parker, G. G., Acker, S. A., & Gower, S. T. (2002). Lidar remote sensing of above-ground biomass in three biomes. *Global Ecology and Biogeography*, 11, 393–399.
- Lefsky, M. A., Harding, D., Cohen, W. B., Parker, G., & Shugart, H. H. (1999). Surface Lidar remote sensing of basal area and biomass in deciduous forests of Eastern Maryland, USA—Results of an international survey. *Remote Sensing of Environment*, 67, 83–98.
- Liu, Xiaoye (2008). Airborne LiDAR for DEM generation: Some critical issues. *Progress in Physical Geography*, 32, 31–49.
- Madelaine, C., Péliissier, R., Vincent, G., Molino, J. F., Sabatier, D., Prévost, M. F., et al. (2007). Mortality and recruitment in a lowland tropical rain forest of French Guiana: Effects of soil type and species guild. *Journal of Tropical Ecology*, 23, 277–287.
- Mascaro, J., Detto, M., Asner, G. P., & Muller-Landau, H. C. (2011). Evaluating uncertainty in mapping forest carbon with airborne LiDAR. *Remote Sensing of Environment*, 115, 3770–3774.
- Næsset, E. (1997). Determination of mean tree height of forest stands using airborne laser scanner data. *ISPRS Journal of Photogrammetry and Remote Sensing*, 52, 49–56.
- Næsset, E. (2002). Predicting forest stand characteristics with airborne scanning laser using a practical two-stage procedure and field data. *Remote Sensing of Environment*, 80, 88–99.
- Næsset, E. (2009). Effects of different sensors, flying altitudes, and pulse repetition frequencies on forest canopy metrics and biophysical stand properties derived from small-footprint airborne laser data. *Remote Sensing of Environment*, 113, 148–159.
- Paget, D. (1999). *Etude de la diversité spatiale des écosystèmes forestiers guyanais. Réflexion méthodologique et application*: ENGREF.
- Poncy, O., Sabatier, D., Prévost, M.-F., & Hardy, I. (2001). The lowland high rainforest: structure and tree species diversity. In P. C.-D. Frans Bongers, Pierre-Michel Forget, & Marc Théry (Eds.), *Nouragues—Dynamics and plant–animal interactions in a Neotropical rainforest* (pp. 416). Dordrecht/Boston/London: Kluwer Academic.
- Saatchi, S. S., Harris, N. L., Brown, S., Lefsky, M., Mitchard, E. T. A., Salas, William, et al. (2011). Benchmark map of forest carbon stocks in tropical regions across three continents. *PNAS*, 108, 9899–9904.
- Sabatier, D., Blanc, L., Bonal, D., Couteron, P., Domenach, A.-M., Frey, V., et al. (2007). Evaluation multi-échelles de la diversité spécifique, structurale et fonctionnelle des arbres en forêt guyanaise : Prise en compte du substrat géologique, des sols et de la dynamique sylvigénétique, ou Diversité Multi-Echelles (DIME). Montpellier: Institut de Recherches pour le Développement—Ministère de l'Ecologie et du Développement Durable.
- Sabatier, D., Grimaldi, M., Prévost, M.-F., Guillaume, J., Gordon, M., Dosso, M., et al. (1997). The influence of soil cover organization on the floristic and structural heterogeneity of a Guianan rain forest. *Plant Ecology*, 131, 81–108.

- Sarrailh, J. M., de Foresta, H., Maury-Lechon, G., & Prévost, M. F. (1990). La régénération après coupe papetière: Parcelle ArboceI. In J. M. Sarrailh (Ed.), *Mise en valeur de l'écosystème forestier guyanais* (pp. 187–208). Inra-Ctft.
- Sun, G., Ranson, K. J., Guo, Z., Zhang, Z., Montesano, P., & Kimes, D. (2011). Forest biomass mapping from lidar and radar synergies. *Remote Sensing of Environment*, 115, 2906–2916.
- Tassi, P. (1989). *Méthode statistiques*. Paris: Economica. Single volume 474 pages.
- Toriola, D., Chareyre, P., & Buttler, A. (1998). Distribution of primary forest plant species in a 19-year old secondary forest in French Guiana. *Journal of Tropical Ecology*, 14, 323–340.
- Vieilledent, G., Vaudry, R., Andriamanohisoa, S. F. D., Rakotonarivo, S. O., Randrianasolo, Z. H., Razafindrabe, H. N., et al. (2011). A universal approach to estimate biomass and carbon stock in tropical forests using generic allometric models. *Ecological Applications*, 22, 572–583.
- Vincent, G., Weissenbacher, E., Sabatier, D., Blanc, L., Proisy, C., & Couteron, P. (2010). Détection des variations de structure de peuplements en forêt dense tropicale humide par Lidar aéroporté (Small foot-print airborne LiDAR proves highly sensitive to changes in structure of moist tropical forest). *Revue Française de Photogrammétrie et Télédétection*, 191, 42–50.
- Wallach, D., & Genard, M. (1998). Effect of uncertainty in input and parameter values on model prediction error. *Ecological Modelling*, 105, 337–345.
- Wright, S. J. (2010). The future of tropical forests. *Annals of the New York Academy of Sciences*, 1195, 1–27.
- Zwally, H. J., Schutz, B., Abdalati, W., Abshire, J., Bentley, C., Brenner, A., et al. (2002). ICESat's laser measurements of polar ice, atmosphere, ocean, and land. *Journal of Geodynamics*, 34, 405–445.